J. Phys.: Condens. Matter **8** (1996) 10799–10821. Printed in the UK

Depletion effects in binary hard-sphere fluids

Thierry Biben†§, Peter Bladon‡ and Daan Frenkel†

† FOM-Institute for Atomic and Molecular Physics (AMOLF), Kruislaan 407, 1098 SJ Amsterdam, The Netherlands

‡ Department of Physics and Astronomy, James Clerk Maxwell Building, King's Buildings, The University of Edinburgh, Mayfield Road, Edinburgh EH9 3JZ, UK

Received 24 July 1996

Abstract. We report a molecular dynamics computation of the entropic depletion force induced between two large spheres (colloidal particles) immersed in a fluid of small spheres. The effective pair potential obtained by numerical integration of the force is used in a Monte Carlo study of the phase behaviour of the binary mixture. The simulation results are compared with the relevant theoretical predictions that follow from various integral equations for liquid mixtures. The simulations provide evidence for a spinodal instability in a liquid mixture of hard spheres with a size ratio of 0.1.

1. Introduction

Depletion forces arise when small particles (polymer, small colloidal particles) are added to a suspension of large colloidal particles. These forces result from the excluded-volume interaction between a large and a small particle. If σ_s denotes the diameter of the small particles and σ_l represents the diameter of the large component, then there is a volume of radius $\xi = (\sigma_s + \sigma_l)/2$ around every large colloidal particle where the centres of the small particles cannot penetrate. The key point is that, although the large particles themselves cannot overlap, the volumes that they exclude for the small components can. As a result, when two large colloidal particles are separated by less than σ_s, the pressure exerted by the small component is anisotropic, leading to a strong attractive force between colloids. In 1958, Asakura and Oosawa [1] suggested that such a depletion mechanism was responsible for the reversible flocculation observed in colloid–polymer mixtures. Their model was based on an excluded-volume calculation, carried out to first order in the density of the small component. They showed that at small separation (smaller than σ_s) there is an attractive interaction between the large colloids. Recently, Mao *et al* [2] extended this calculation by taking into account the second- and the third-order contribution of the small-particle density to the depletion force. They found evidence for a pronounced repulsive barrier close to the attractive depletion well when the separation between colloids is larger than σ_s. The presence of such a repulsive interaction in the potential of mean force of two colloidal spheres is qualitatively similar to the oscillating force between the solid surfaces that confine a thin layer of liquid [3]. The characteristic distance scale of these oscillations is determined by the size of the confined molecules (in the present case, the small particles). Such oscillations are due to the layering of the confined fluid close to the surfaces. In

§ Permanent address: Laboratoire de Physique (Unité de Recherche Associée 1325 du CNRS), Ecole Normale Supérieure de Lyon, 69364 Lyon Cèdex 07, France.

0953-8984/96/5010799+23$19.50

section 3, we show that in a molecular dynamics (MD) study of the depletion force such oscillating behaviour is indeed observed.

At this stage it is important to define more accurately what we mean by 'the depletion force'. Mixtures of small and large colloidal particles are often modelled as a mixture of dissimilar hard spheres. For instance, the calculations by Mao *et al* [2] are based on such a model. But colloid–polymer mixtures cannot be accurately modelled by a mixture of hard spheres, since the interaction between polymers is usually quite weak. This aspect is captured by the Asakura–Oosawa model which assumes a *non-additive* hard-sphere interaction where polymers can interpenetrate each other freely. If we denote the contact distance between two particles of species 'A' ('B') by σ_{AA} (σ_{BB}), then for non-additive hard spheres, the contact distance between particles 'A' and 'B' is defined as

$$\sigma_{AB} = \frac{\sigma_A + \sigma_B}{2}(1 + \Delta) \tag{1}$$

where Δ is the non-additivity parameter. When $\Delta < 0$, particles 'A' and 'B' 'like' each other, so mixing is favoured. In contrast, when $\Delta > 0$, which is the case of polymer–colloid mixtures, particles 'A' and 'B' prefer not to mix, with the result that phase separation can occur. Many studies of non-additive hard-sphere fluids have been performed for equally sized particles [4], while large size ratios have been investigated in reference [5] using an equation of state suggested by Barboy and Gelbart [6]. It appears from this study that for large size ratios, non-additivity is the leading contribution to phase separation. The case of a purely additive hard-sphere mixture ($\Delta = 0$) is of considerable practical relevance, yet very special from a theoretical point of view. In what follows, we focus on this case. We will show that the competition between the entropy of the large and the smaller particles is very subtle. It results in a slow phase separation of the two components, preceded by the formation of clusters of large spheres.

Before we consider the phase behaviour of hard-sphere mixtures, we first briefly review some of the published theoretical results on the pair structure. We present Monte Carlo (MC) simulation data that allow us to test these theoretical predictions in considerable detail (section 2). Subsequently, we consider in more detail the effective pair interactions between the large colloidal particles immersed in a reservoir of small spheres (section 3). In section 4 we use the effective pair potential, as determined by MD simulations, as input for Monte Carlo simulations to study the behaviour of a fluid of hard spheres interacting through a short-ranged depletion interaction (section 4).

2. Integral equations versus simulations

2.1. Introduction

Pair correlations in a fluid provide a quantitative measure of both the local order, i.e. the way in which molecules are organized in the neighbourhood of a given molecule of the fluid, and the long-range order. Local properties show up most clearly in the pair distribution function itself, while long-range properties, such as the compressibility, appear more clearly in Fourier space, i.e. in the structure factor. The usual starting point for the theoretical calculation of pair correlation functions in liquids is the well known Ornstein–Zernike equations [7]:

$$h_{\alpha\beta}(r) = c_{\alpha\beta}(r) + \sum_{\gamma} \rho_\gamma c_{\alpha\gamma}(r) * h_{\gamma\beta}(r) \tag{2}$$

where $h_{\alpha\beta}(r)$ is the pair correlation function for particles of species α and β respectively. This pair correlation function is related to the pair distribution function $g_{\alpha\beta}(r)$ through the

simple equation $h_{\alpha\beta}(r) = g_{\alpha\beta}(r) - 1$. $c_{\alpha\beta}(r)$ is the Ornstein–Zernike direct correlation function, and ρ_α is the number density of 'α'-particles. '$*$' denotes a convolution. It is clear that equations (2) do not constitute a closed system, and a set of closure relations is necessary to compute both $g(r)$s and $c(r)$s. Every closure of equation (2) leads to an integral equation for $g(r)$. The search for good approximate closure relations of equation (2) has resulted in a large number of such integral equations. For hard-sphere mixtures, the first successful integral equation was the famous Percus–Yevick equation [8]. However, more recent integral equations, such as the ones that result from the closures proposed by Rogers and Young (RY) [9] and by Ballone, Pastore, Galli and Gazzillo (BPGG) [10], have proven to provide a more accurate estimate of the pair structure of a hard-sphere fluid, in particular at high densities. Introducing the notation $\gamma_{\alpha\beta}(r) = h_{\alpha\beta}(r) - c_{\alpha\beta}(r)$, the PY, RY and BPGG closure relations take the forms

$$g_{\alpha\beta}(r) = \exp(-\beta U_{\alpha\beta}(r))[1 + \gamma_{\alpha\beta}(r)] \qquad \text{(PY)} \tag{3}$$

where $U_{\alpha\beta}(r)$ is the pair potential between a particle of type 'α' and a particle of type 'β' (the factor β appearing in the exponential is the inverse temperature $\beta = 1/k_B T$),

$$g_{\alpha\beta}(r) = \exp(-\beta U_{\alpha\beta}(r))\left[1 + \frac{\exp(\gamma_{\alpha\beta}(r) f_{\alpha\beta}(r)) - 1}{f_{\alpha\beta}(r)}\right] \qquad \text{(RY)} \tag{4}$$

where the function $f_{\alpha\beta}(r) \equiv 1 - \exp(-\xi_{\alpha\beta} r)$ varies between 0 and 1, and finally

$$g_{\alpha\beta}(r) = \exp(-\beta U_{\alpha\beta}(r)) \exp\{[1 + s\gamma_{\alpha\beta}(r)]^{1/s} - 1\} \qquad \text{(BPGG).} \tag{5}$$

In the latter two expressions, additional adjustable parameters occur, namely '$\xi_{\alpha\beta}$' for the RY closure and 's' for the BPGG approximation. However, these parameters cannot be chosen at will, as they should be chosen such that they eliminate the so-called thermodynamical inconsistency that plagues many approximate integral equations, such as the PY one. A manifestation of this inconsistency is that there is a difference between the pressure as computed from the virial equation of state, and as computed from the compressibility relation. A detailed discussion of these integral equations applied to a very asymmetric mixture of hard spheres can be found in reference [11], and partially in references [12–14]. We briefly summarize the most important theoretical predictions in the next section, and present a comparison with the results of numerical simulations for a size ratio $y = \sigma_s/\sigma_l = 0.1$. But before we discuss the results, we briefly comment on the MC simulation technique.

In standard MC simulations, new configurations are generated by attempting to displace individual particles over a small, but otherwise random distance. If this trial move results in an overlap, the move is rejected. The average size of the trial displacement must not be too small, otherwise the new configuration does not differ significantly. Neither should the displacement be too large, because then the probability of overlap is so high that the move is almost always rejected. In order to get a reasonable acceptance, the magnitude of a trial move should be of the order of the typical surface-to-surface separation between particles. In the case of large spheres immersed in a concentrated suspension of small particles, the mean separation between the surfaces of two particles is typically a fraction of the diameter of the *smallest* component. As a result, the displacement of a large particle cannot exceed the scale of a small particle. In fact, the situation is worse, as one large particle can overlap with many small particles simultaneously. And any one such overlap is sufficient to lead to the rejection of the trial move. As a consequence, the standard MC scheme is very inefficient in moving large particles in a sea of small particles. To perform efficient numerical simulations of highly asymmetric mixtures, we have used a special Monte Carlo

algorithm that allows us to carry out exchanges between small and large particles [11]. This algorithm, that is based on the configurational bias Monte Carlo method [15, 16], is presented in appendix A. Similar algorithms have been used to study mixtures of hard cubes [17, 18] and mixtures of spherical and rod-like colloids [19].

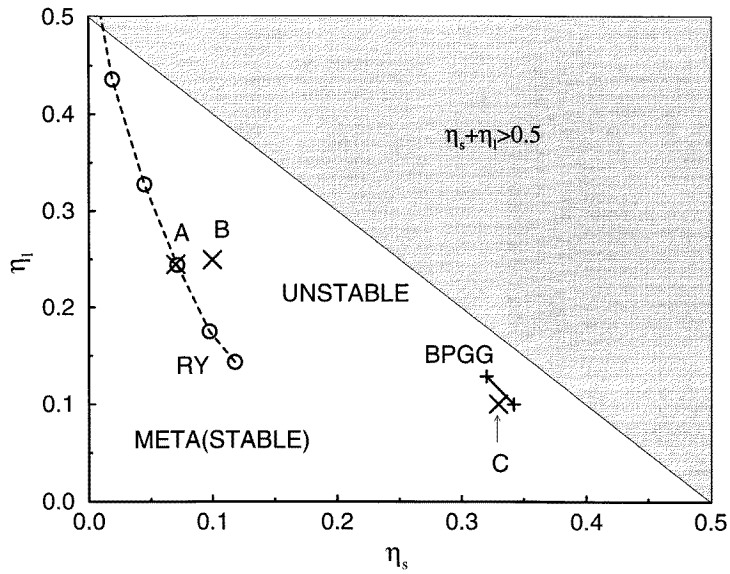

Figure 1. The phase diagram of a hard-sphere binary mixture of size ratio 0.1. The dashed curve corresponds to the spinodal as predicted by the RY approximation. The stable and unstable regions are indicated in the figure. Two points of the BPGG spinodal are also presented. The grey area corresponds to the region $\eta_s + \eta_l > 0.5$, where the system is likely to have solidified. In any event, crystallization is not considered in the integral equations. It is, however, quite likely that crystallization of the large spheres will already have started at a lower overall packing fraction (see the text). The three points A, B and C correspond to the thermodynamical states for which MC computations have been performed.

2.2. Comparison with simulation

Let us briefly summarize the most striking theoretical predictions concerning the behaviour of highly asymmetric hard-sphere mixtures. First of all, the integral equations that we consider all predict that, at fixed packing fraction, the pair distribution function of the large spheres will develop a δ-peak at contact (i.e. at $r = \sigma_l$) [12], in the limit $y = \sigma_s/\sigma_l \to 0$. It has been shown that within the PY approximation, the system of large spheres reduces to the well known Baxter (sticky-sphere) model in this limit [14]. The second interesting theoretical result concerns the possible existence of spinodal instability in the binary fluid mixture. Both the RY and BPGG integral equations [13] predict that such an instability should develop whereas the PY equation always predicts complete miscibility of the two components [20, 21]. Figure 1 shows the predicted phase diagram for a size ratio $y = 0.1$. The figure suggests that there are appreciable differences between the prediction of the two 'thermodynamically self-consistent' integral equations. We now focus on a particular thermodynamical state, chosen close to the RY spinodal line (point 'A' of the phase diagram). For this state point, the packing fractions are respectively $\eta_s (= \pi/6\rho_s\sigma_s^3) = 0.072$

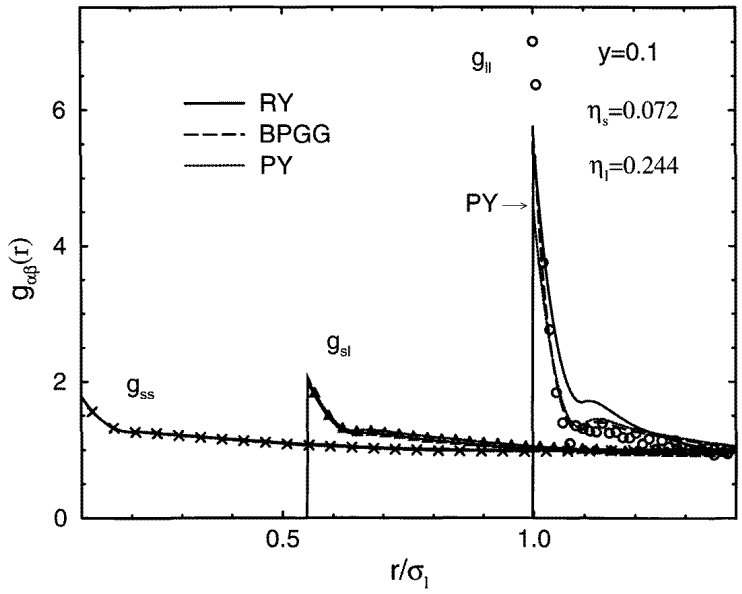

Figure 2. Pair distribution functions for state point 'A'. A comparison between integral equation results and MC data. PY and BPGG predictions are in close agreement with the MC data, except close to the contact value of g_{ll}. The PY contact value is indicated by the arrow. The MC contact value is a based on a linear three-point extrapolation, and is expected to be a lower bound.

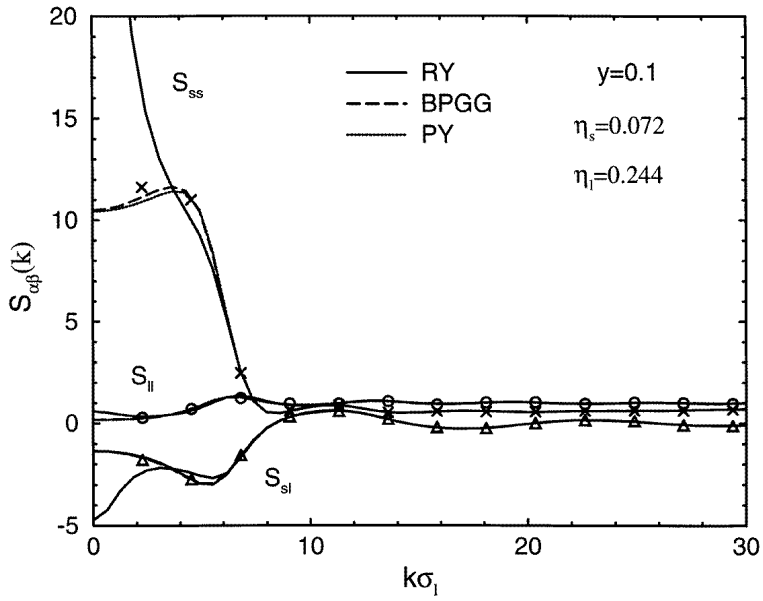

Figure 3. Structure factors for state point 'A'. The large peak that appears in $S_{ss}(k)$ at low values of k is due to the scattering by the network of large colloidal particles. But the extra divergence observed for $k = 0$ within the RY approximation corresponds to a spinodal instability.

for the small particles, and $\eta_l = 0.244$ for the large ones. The choice of this state point was dictated primarily by computational considerations: as the computer time increases strongly with the total number of particles. The number of small particles is related to the number of large ones through the relation $N_s = N_l\eta_s/(\eta_l y^3)$. Even if we fix the number of large particles at a quite small value (say 10) then, for a size ratio $y = 0.1$, the number of small particles is of order 10^4 for $\eta_s/\eta_l = \mathcal{O}(1)$. The region of the phase diagram that we can explore with the MC algorithm presented in appendix A is then the region of large η_l and low η_s. Figure 2 shows a comparison of the Monte Carlo results for the pair distribution functions and the corresponding theoretical predictions. As expected, we observe a large value of g_{ll} at contact. This effect is even stronger in the MC simulations than in the theoretical predictions. A second feature to note is the slow decay of g_{ss} at large distances. The theoretical interpretation of this behaviour is discussed in some detail in reference [12]: it is due to the fact that, in the limit $y \to 0$ and at fixed packing fractions, the fluid of small particles behaves like an effective fluid placed in a network of cavities made by the large particles. The bulk density of this effective fluid is simply $\rho_s^* = \rho_s/(1-\eta_l)$, due to the reduction of the accessible volume. The slow variation of g_{ss} is a consequence of the Gruyere-like structure of this effective fluid. As a consequence, the structure factor $S_{ss}(k)$ exhibits a peak at small values of k, due to the scattering by the network of cavities. We can observe this effect in figure 3. It is interesting to note that the BPGG and even the PY equation predict a behaviour of $S_{ss}(k)$ that is in close agreement with the simulations. However, the RY equation predicts large fluctuations at $k = 0$ for $S_{ss}(k)$ close to the spinodal line, in contradiction to the simulation results. We return to a discussion of the behaviour of g_{ss} in section 3.

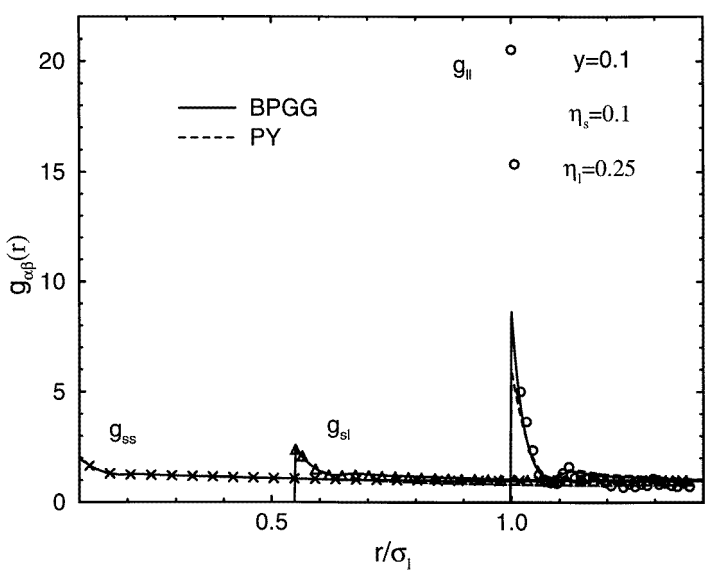

Figure 4. Pair distribution functions for state 'B'. Note the very large contact value of g_{ll} obtained in MC simulation.

Next, we consider state point 'B' of the phase diagram shown in figure 1 ($\eta_s = 0.1$, $\eta_l = 0.25$). As can be seen in figures 4 and 5, the situation now is very different. For point 'B', we do not have the results for the RY closure, as this state point is in the unstable region of the RY phase diagram. However, the MC results now exhibit behaviour that resembles

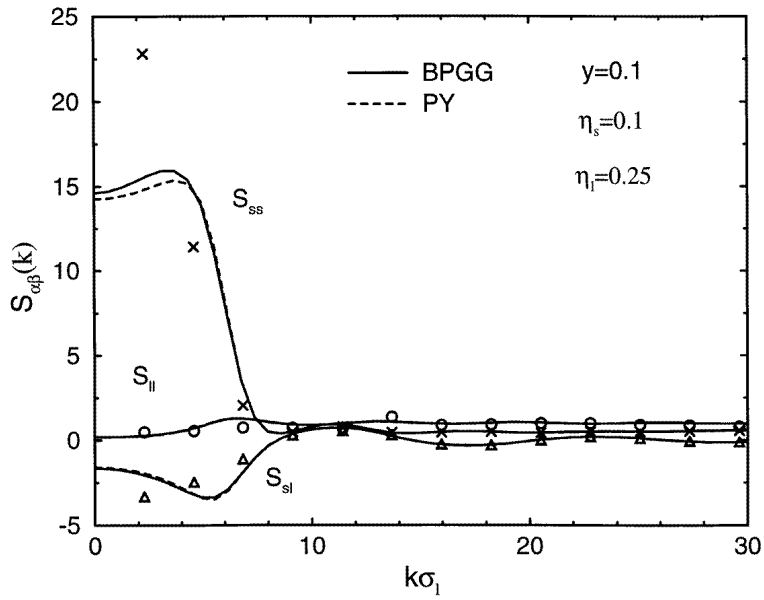

Figure 5. Structure factors for state 'B'. MC data differ from BPGG and PY estimates, and exhibit the same behaviour as RY data close to the spinodal line. However, the RY integral equation has no solution for this state point.

the results of the RY approximation for state 'A'. The proximity of a spinodal line is also suggested by the very large contact value of g_{ll} (>20) found in the MC simulation of point 'B'.

2.3. Discussion

The previous results, especially those obtained for state point 'B', suggest that there is indeed a spinodal instability in the hard-sphere fluid mixture. However, it should be noted that the numerical simulations for state point 'B' are less accurate than for point 'A'. The reason is that at point 'B', the density of small spheres is a factor of 1.4 higher than at point 'A'. As the efficiency of the insertion method discussed in appendix A decreases rapidly with increasing density, the acceptance rate for trial moves of the large spheres is much less at point 'B' than at point 'A'. As a result, the statistical errors in the simulation results at point 'B' are quite large and this makes it difficult to make categorical statements about the occurrence of a phase separation. Apart from that, it is encouraging to note the good overall agreement with the MC simulation results of the predictions based on the BPGG approximation (and on the RY approximation, far from any spinodal line). To extend the test of the theories to other parts of the phase diagram, it is necessary to increase both the size of the system (the above MC simulations were performed with $N_l = 10$!), and to increase the packing fraction of the small particles. Under those conditions, the MC simulations of the type described above, although more efficient than conventional MC simulations, are nevertheless prohibitively expensive. To gain insight into the phase behaviour in this regime, we try to map the mixture of large particles immersed in a bath of small particles onto an effective one-component fluid interacting through an effective potential. Once we have determined the effective pair potential, we can limit our simulations to the large particles

only. It should be stressed that such an approach is only justified if the potential of mean force is pairwise additive. In the limit $y \to 0$, this is indeed the case.

3. The effective potential

3.1. The general expressions for the potential and for the mean force

When large particles, such as colloids, are immersed into a suspension of particles that are much smaller, it is tempting to describe the interactions between the large particles in terms of an effective potential. The standard statistical-mechanical approach for arriving at such a simplified description is to integrate the full Boltzmann factor of the system over all degrees of freedom of the suspending fluid. The mean value of a dynamical variable A in the canonical ensemble is defined by

$$\langle A(\{\boldsymbol{X}_I, \boldsymbol{P}_I\})\rangle = \frac{1}{Z}\int \prod_I \mathrm{d}\boldsymbol{X}_I\ \mathrm{d}\boldsymbol{P}_I \prod_i \mathrm{d}\boldsymbol{x}_i\ \mathrm{d}\boldsymbol{p}_i\ A(\{\boldsymbol{X}_I, \boldsymbol{P}_I\}) \times \exp\left[-\beta\left(\sum_I \frac{\boldsymbol{P}_I^2}{2M} + \sum_{I<J} V_{IJ} + \sum_i \frac{\boldsymbol{p}_i^2}{2m} + \sum_{i<j} V_{ij} + \sum_{iI} V_{iI}\right)\right] \tag{6}$$

with the convention that capital letters represent quantities related to colloidal particles. V_{ij} represents the interaction between a pair of small particles; V_{iI} represents the interaction between the small and the large particles; and V_{IJ} represents the interaction between two colloidal (i.e. large) particles. $\beta = 1/k_B T$ is the inverse temperature, and Z is the partition function:

$$Z = \int \prod_I \mathrm{d}\boldsymbol{X}_I\ \mathrm{d}\boldsymbol{P}_I \prod_i \mathrm{d}\boldsymbol{x}_i\ \mathrm{d}\boldsymbol{p}_i\ \exp\left[-\beta\left(\sum_I \frac{\boldsymbol{P}_I^2}{2M} + \sum_{I<J} V_{IJ} + \sum_i \frac{\boldsymbol{p}_i^2}{2m} + \sum_{i<j} V_{ij} + \sum_{iI} V_{iI}\right)\right]. \tag{7}$$

Equation (6) can easily be rewritten:

$$\langle A(\{\boldsymbol{X}_I, \boldsymbol{P}_I\})\rangle = \frac{1}{\mathcal{Z}}\int \prod_I \mathrm{d}\boldsymbol{X}_I\ \mathrm{d}\boldsymbol{P}_I\ A(\{\boldsymbol{X}_I, \boldsymbol{P}_I\}) \times \exp\left[-\beta\left(\sum_I \frac{\boldsymbol{P}_I^2}{2M} + \sum_{I<J} V_{IJ} + \mathcal{V}(\{\boldsymbol{X}_I\})\right)\right] \tag{8}$$

where the effective potential $\mathcal{V}$ is defined by

$$\beta\mathcal{V}(\{X_I\}) = -\ln\left\{\int \prod_i \mathrm{d}\boldsymbol{x}_i\ \exp\left[-\beta\left(\sum_{iI} V_{iI} + \sum_{i<j} V_{ij}\right)\right]\right\} \tag{9}$$

and the effective partition function is

$$\mathcal{Z} = \int \prod_I \mathrm{d}\boldsymbol{X}_I\ \mathrm{d}\boldsymbol{P}_I\ \exp\left[-\beta\left(\sum_I \frac{\boldsymbol{P}_I^2}{2M} + \sum_{I<J} V_{IJ} + \mathcal{V}(\{\boldsymbol{X}_I\})\right)\right]. \tag{10}$$

Obviously, the effective potential is a complicated object that depends on all the coordinates of all the colloidal particles. In order to simplify matters, it is convenient to introduce the mean force acting on a colloidal particle. This mean force is defined as (minus) the gradient

of the effective potential with respect to the position of the particle. Using equation (9), the mean force acting on a colloidal particle with index K is given by

$$-\boldsymbol{\nabla}_{\boldsymbol{X}_K}\{\mathcal{V}(\{X_I\})\} = -\sum_l \int \left\{ \int \prod_{i\neq l} \mathrm{d}\boldsymbol{x}_i \ \exp\left[-\beta\left(\sum_{iI} V_{iI} + \sum_{i<j} V_{ij}\right)\right]\right\} \times \left\{ \int \prod_i \mathrm{d}\boldsymbol{x}_i \ \exp\left[-\beta\left(\sum_{iI} V_{iI} + \sum_{i<j} V_{ij}\right)\right]\right\}^{-1} \boldsymbol{\nabla}_{\boldsymbol{X}_K}\left(V_{lK}\right) \mathrm{d}\boldsymbol{x}_l \tag{11}$$

where the notation $\boldsymbol{\nabla}_{\boldsymbol{X}_K}$ denotes the gradient with respect to the position $\boldsymbol{X}_K$ of the colloidal particle, and the sum is taken over the small particles (index 'l'). We easily recognize in this last expression the single-particle density of the small particles in the external field of the large ones:

$$\rho^{(1)}(\boldsymbol{x}_l|\{X_I\}) \equiv N_s \left\{ \int \prod_{i\neq l} \mathrm{d}\boldsymbol{x}_i \ \exp\left[-\beta\left(\sum_{iI} V_{iI} + \sum_{i<j} V_{ij}\right)\right]\right\} \times \left\{ \int \prod_i \mathrm{d}\boldsymbol{x}_i \ \exp\left[-\beta\left(\sum_{iI} V_{iI} + \sum_{i<j} V_{ij}\right)\right]\right\}^{-1}. \tag{12}$$

The mean force then reads

$$\mathcal{F}_K(\{\boldsymbol{X}_I\}) = -\frac{1}{N_s}\sum_l \int \mathrm{d}\boldsymbol{x}_l \ \boldsymbol{\nabla}_{\boldsymbol{X}_K}(V_{lK})\rho^{(1)}(\boldsymbol{x}_l|\{X_I\}). \tag{13}$$

Because the interaction potential V_{lK} depends only on $\boldsymbol{x}_l - \boldsymbol{X}_K$, we have $\boldsymbol{\nabla}_{\boldsymbol{X}_K}(V_{lK}) = -\boldsymbol{\nabla}_{\boldsymbol{x}_l}(V_{lK})$. The sum over the small particles then reduces to a factor of N_s. The final expression of the mean force is simply

$$\mathcal{F}_K(\{\boldsymbol{X}_I\}) = \int \mathrm{d}\boldsymbol{r} \ \boldsymbol{\nabla} V_{sl}(r)\rho^{(1)}(\boldsymbol{r}|\{X_I\}) \tag{14}$$

where $V_{sl}(r)$ is the pair interaction between a large and a small particle (assumed to be spherically symmetric for the sake of simplicity). Here, $\rho^{(1)}(\boldsymbol{r}|\{X_I\})$ is the equilibrium single-particle density of the small particles in the external field of the large ones, with the convention that particle K is placed at the origin. For hard-sphere interactions, the effective mean force is

$$\beta\mathcal{F}_K(\{X_I\}) = \xi^2 \int \mathrm{d}\hat{\boldsymbol{\sigma}} \ \rho^{(1)}(-\xi^+\hat{\boldsymbol{\sigma}}|\{\boldsymbol{X}_I\})\hat{\boldsymbol{\sigma}} \tag{15}$$

where $\xi = (\sigma_s + \sigma_l)/2$ is the radius of the pair excluded volume (σ_s and σ_l are the diameters of small and large particles respectively). $\hat{\boldsymbol{\sigma}}$ is a unit vector, pointing towards the centre of the large sphere. The integral is then calculated just outside the surface of the excluded volume associated with colloidal particle 'K'. The interpretation of equation (15) is very simple: the mean force acting on colloidal particle 'K' is simply the surface integral of the normal component of the instantaneous local pressure at the surface of this particle. Of course, the above 'derivation' is static in nature and says nothing about the time-scale on which this mean force is a meaningful concept. It is therefore interesting to note that equation (15) has also been derived from a multiple-time-scale analysis of kinetic theory in reference [22].

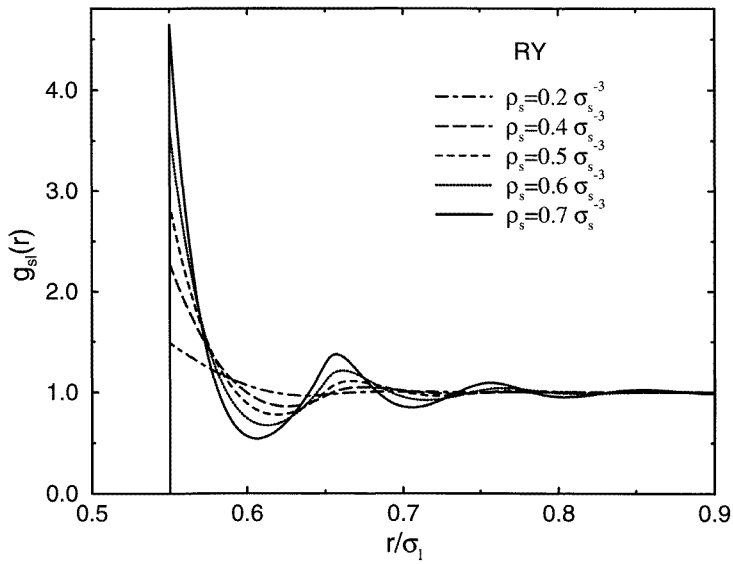

Figure 6. The predicted density dependence of the distribution of the small particles around a large sphere (size ratio $y = 0.1$). The radial distribution functions were computed using the Rogers–Young integral equation.

3.2. Pairwise additivity of the mean force

Let us first consider the situation where a finite number of large spheres, say N_l, are placed in an infinite volume filled with small spheres at a density ρ_s. In this case the density of large particles $\rho_l = 0$. If there is only one large particle in the fluid formed by the small ones, the mean force is obviously zero since the distribution of the smaller particles around the large one is isotropic. When two large particles are at a distance 'd', the effective force between them can be measured directly using molecular dynamics (MD) simulations. Alternative, the force may be estimated using the superposition approximation:

$$\rho^{(1)}(\boldsymbol{x}|\boldsymbol{X}_1, \boldsymbol{X}_2) \simeq \rho_s g_{sl}(\boldsymbol{x} - \boldsymbol{X}_1) g_{sl}(\boldsymbol{x} - \boldsymbol{X}_2) \tag{16}$$

where g_{sl} is the small–large pair distribution function of the binary mixture at infinite dilution of the large spheres. This pair distribution function can be estimated using an integral equation, such as the Percus–Yevick or Rogers and Young (RY) ones. Figure 6 shows the Rogers-Young prediction for the density dependence of g_{sl}. In the superposition approximation, the force acting on particle '1' can be written as

$$\beta \mathcal{F}_1(\boldsymbol{X}_1, \boldsymbol{X}_2) = \xi^2 \rho_s g_{sl}(\xi) \int \mathrm{d}\hat{\boldsymbol{\sigma}}\ \hat{\boldsymbol{\sigma}} h_{sl}(\boldsymbol{X}_2 - \boldsymbol{X}_1 + \xi \hat{\boldsymbol{\sigma}}) \tag{17}$$

where we have introduced the pair correlation function $h_{sl}(r) = g_{sl}(r) - 1$, that goes to zero at large distances.

A comparison of simulation data and the superposition approximation using both PY and RY approximations is shown in figure 7. This figure shows that for densities as large as $\rho_s = 0.4\sigma_s^{-3}$ the superposition approximation yields an excellent estimate of the pair force. At higher densities we observe a phase shift of the oscillations close to the repulsive peak, but far from this peak ($d = 3\sigma_s$) the superposition approximation works well, as

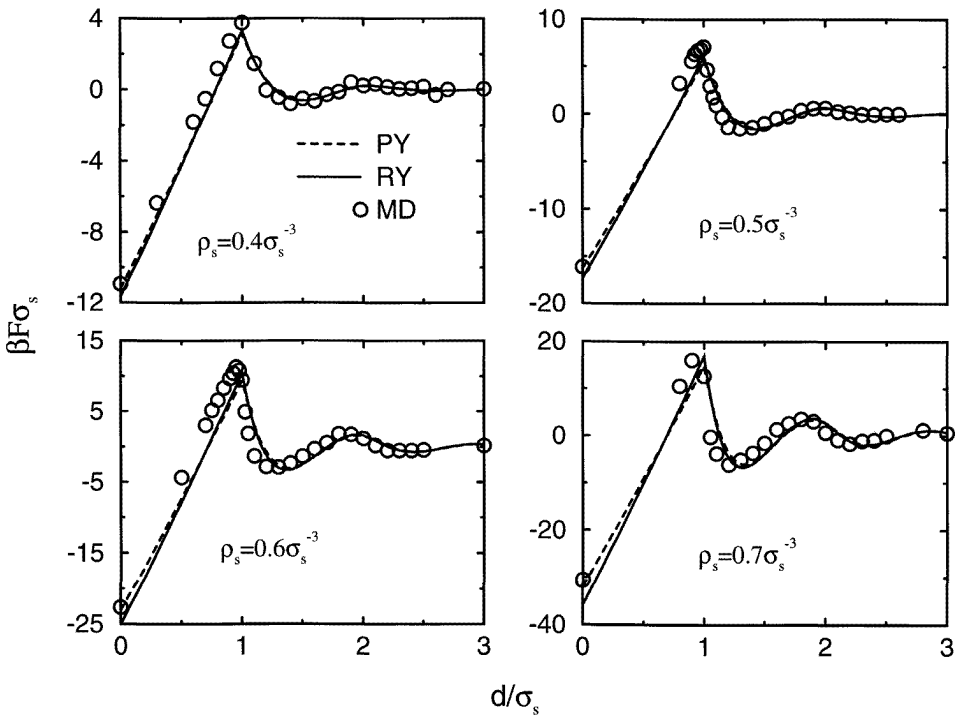

Figure 7. The depletion force as measured during a MD simulation. A comparison with the superposition approximation, using the PY or RY approximation for $g_{sl}(r)$. Even though discrepancies occur at high densities and short distances, the agreement is quite good at large distances.

expected. This success of the superposition approximation in predicting the distribution of small particles around two spheres has been pointed out earlier by Attard [23].

When more than two colloidal particles are present, there is no *a priori* reason for the force to be pairwise additive. If we consider the particular case of three large spheres, it is easy to show that the three-particle superposition approximation leads to

$$\beta\mathcal{F}_1(\{X_I\}) = \xi^2\rho_s g_{sl}(\xi)\int \mathrm{d}\hat{\boldsymbol{\sigma}}\ \hat{\boldsymbol{\sigma}}\left(\sum_{I=2,3} h_{sl}(\boldsymbol{X}_I - \boldsymbol{X}_1 + \xi\hat{\boldsymbol{\sigma}}) + \prod_{I=2,3} h_{sl}(\boldsymbol{X}_I - \boldsymbol{X}_1 + \xi\hat{\boldsymbol{\sigma}})\right). \tag{18}$$

Using equation (17), we can rewrite equation (18) as

$$\beta\mathcal{F}_1(\boldsymbol{X}_1, \boldsymbol{X}_2, \boldsymbol{X}_3) = \beta\mathcal{F}_1(\boldsymbol{X}_1, \boldsymbol{X}_2) + \beta\mathcal{F}_1(\boldsymbol{X}_1, \boldsymbol{X}_3) + \xi^2\rho_s g_{sl}(\xi)\int \mathrm{d}\hat{\boldsymbol{\sigma}}\ \hat{\boldsymbol{\sigma}}\prod_{I=2,3} h_{sl}(\boldsymbol{X}_I - \boldsymbol{X}_1 + \xi\hat{\boldsymbol{\sigma}}). \tag{19}$$

This last expression shows that the breakdown of pairwise additivity comes from the overlap of the pair correlation functions around particles '2' and '3' on the surface of the excluded sphere of radius ξ around particle '1'. However, figure 6 shows that the typical range of the pair correlation function $h_{sl}(r)$ is of the order of $\xi + 3\sigma_s$, which means that the correction

to pairwise additivity only appears when all three spheres are very close together. To get a feeling for the magnitude of this effect, consider the particular (and extreme) case where particle 1 is in contact with both particle 2 and particle 3, while θ is the angle $\widehat{213}$.

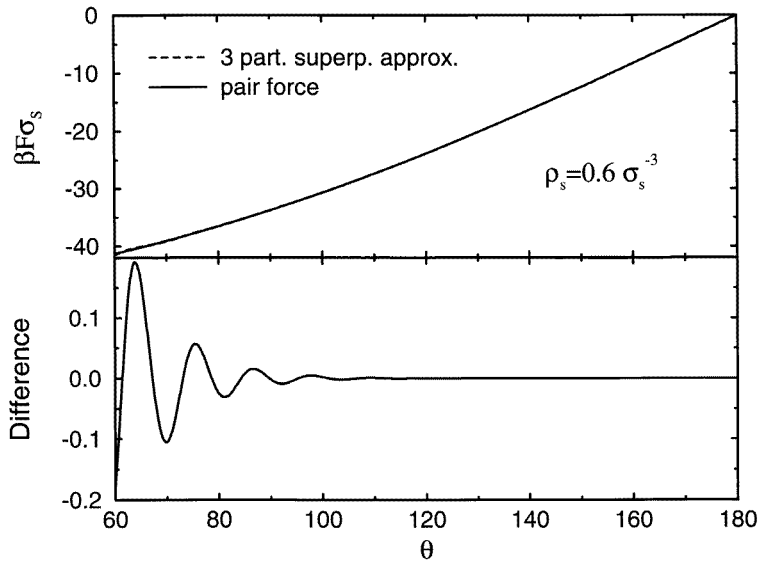

Figure 8. The three-particle superposition approximation versus pairwise estimation of the force. The top curve represents the force acting on a central particle at contact with two other particles. θ is the angle between the vectors joining the central sphere to these two particles. We only notice a very small difference when the three particles are close to contact ($\theta = 60°$). The bottom curve is the difference between the two previous curves. *Note the difference in scale between the top and bottom figures.*

Figure 8 shows two different estimates of the net force on particle 1. The first estimate was obtained using the three-particle superposition approximation. And the second estimate was computed assuming pairwise additivity of the forces. The angle θ was varied between 60° (all three particles in contact) and 180° (collinear configuration). The size ratio σ_s/σ_l was 0.1. As can be seen in figure 8, even for highly packed configurations the pairwise-additivity approximation yields excellent results, even close to the triangular configuration and for a rather high density of small particles ($0.6\sigma_s^{-3}$).

The reason is twofold. First of all, for small values of the size ratio y, the range of $h_{sl}(r)$ is small compared to the size of the large particles. Secondly, for size ratios less than 0.154, there are no 'triply excluded' configurations of the small sphere, i.e. there are no configurations for which the small sphere could overlap with all three large spheres simultaneously. This removes another obvious source of non-pairwise-additive effects in the depletion interaction. It therefore seems reasonable to assume that for a size ratio $y = 0.1$ (or less), the depletion interaction is, to a good approximation, pairwise additive, even for concentrated colloidal systems. We stress that this pairwise additivity is expected to break down for larger values of the size ration.

The density ρ_s that appears in equation (16) is the density of the suspension of small particles *far from* the two colloidal particles. However, this is only true at infinite dilution of the large spheres. For finite values ρ_l, the bulk density of the small spheres that enters into the superposition approximation is no longer $\rho_s = N_s/V$, as the volume V_{acc} that is

accessible to the small particles is reduced by the presence of the large particles. However, the density of the small particles as such is not the quantity of interest. What we need to know are the structural properties of a suspension of small particles in osmotic equilibrium with the mixture. In the case where the concentration of large particles in the mixture tends to zero, the density of the small particles in the mixture is equal to their density in the reservoir. However, in general the densities will be different. To give a specific example, consider the case where the size ratio $\sigma_s/\sigma_l \to 0$. In this case, the fraction of the volume in the mixture that is accessible to small particles is simply $V_{acc}/V = 1 - \eta_l$, where η_l is the packing fraction of the large particles. And hence the density of small particles in the mixture (ρ_s) is related to the density in the reservoir (ρ_s^*) through

$$\frac{\rho_s}{1-\eta_l} = \rho_s^*. \tag{20}$$

In the more general case, the relation between the densities is fixed by the condition of osmotic equilibrium (i.e. equal chemical potentials). In the limit where $\rho_s \to 0$, the relation between the density of small particles in the reservoir and in the mixture is given by the Widom relation [24]:

$$\rho_s = \rho_s^* \exp[-\beta\mu_s^{ex}(\rho_l, \rho_s = 0)] \tag{21}$$

where μ_s^{ex} denotes the excess chemical potential of the small particles in the mixture. An approximate relation between ρ_s and ρ_s^* can be obtained for hard spheres using scaled particle theory [25, 26]:

$$\rho_s^* = \frac{\rho_s}{1-\eta_l} \exp\left[\frac{3\eta_l}{1-\eta_l}y + \frac{3\eta_l}{(1-\eta_l)^2}\left(1+\frac{\eta_l}{2}\right)y^2 + \frac{\eta_l+\eta_l^2+\eta_l^3}{(1-\eta_l)^3}y^3\right] \tag{22}$$

where $y = \sigma_s/\sigma_l$. We shall assume that this relation also holds for finite ρ_s.

3.3. The effective pair potential

The pair potential of mean force can be obtained by integration from the average force itself:

$$\beta V(r_s) = \int_{r_s}^{+\infty} \beta\mathcal{F}(r_s')\sigma_s \, \mathrm{d}r_s' \tag{23}$$

where $r_s = r/\sigma_s$ is the dimensionless distance to the centre of the large sphere. The determination of the effective potential using equation (23) and MD data presented in figure 7 is not completely straightforward since we do not have data for separations larger than $3\sigma_s$. However, this problem is not too serious since we know that the superposition approximation is accurate at large separations. We can then estimate the integral of the force between $r_s = \xi/\sigma_s + 3$ and $+\infty$ by using this approximation. In any event, this contribution turns out to be negligible.

It is interesting to compare the computed depletion potential to the perturbation theory prediction of reference [2]. The simulated pair potentials, together with the superposition approximation and the perturbation theory predictions, are shown in figure 9. This figure shows the variation of the depletion potential for different values of ρ_s^*. The results show that the two theories are, in a sense, complementary: at low densities ($\rho_s^* = 0.4\sigma_s^{-3}$) the MD data for the mean force compare well with the superposition approximation (see figure 7), except inside the depletion well (separations smaller than σ_s). At higher densities, the discrepancies propagate to larger separations. In contrast, the perturbation theory of reference [2] accurately reproduces the MD data inside the depletion well, even at relatively

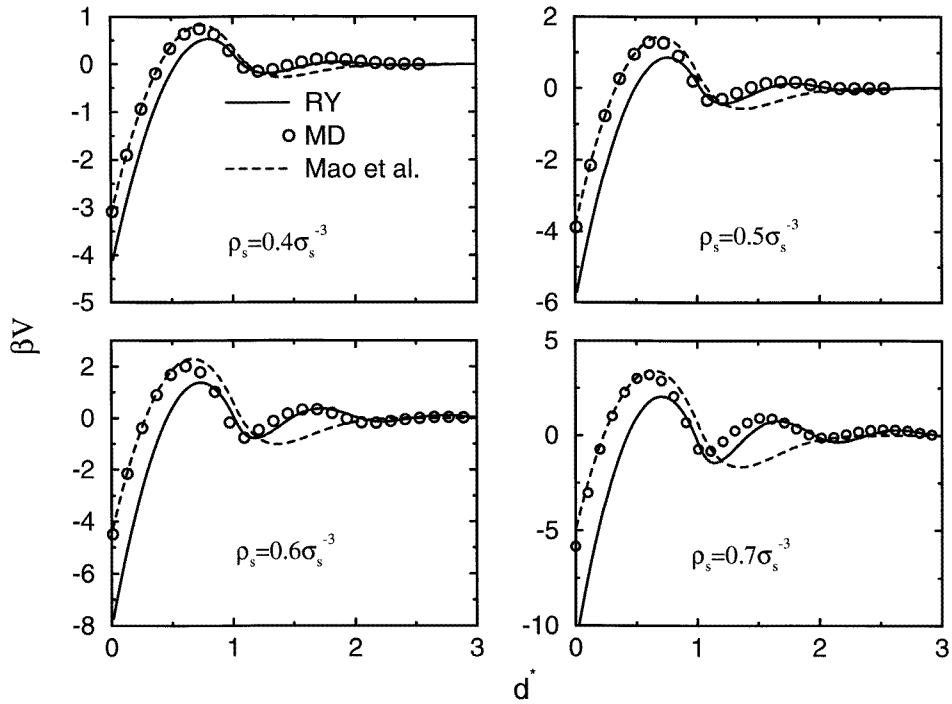

Figure 9. The effective depletion potential as a function of the density of small particles. This figure shows a comparison between MD data, the theory of Mao *et al* [2], and the superposition approximation using the RY pair distribution functions. In every case, the short-distance behaviour coincides with the perturbation theory of reference [2], and the long-range behaviour compares very well with the superposition approximation.

high effective densities. But at larger distances, the oscillations of the potential are only poorly reproduced by the perturbation theory. At low densities, both theories agree with the MD data.

For what follows, we emphasize once again the result presented in figure 8: for a suspension of large spheres immersed in a bath of small spheres (size ratio of 0.1), the force between the large spheres is, to an excellent approximation, pairwise additive, even for quite compact configurations of the large spheres. We therefore assume that, in Monte Carlo simulations, we can use this effective pair potential to represent the effect of the small spheres on the large ones.

4. Simulation of the effective one-component fluid

Simulations were performed on a system of 2700 large colloidal particles interacting through the effective potential discussed above. We stress that this effective potential is a function of the chemical potential of the small particles. The size ratio is fixed at a value of 0.1. A test of this effective one-fluid model is presented in figure 10. In this figure we compare the MC results obtained for the $g_{ll}(r)$ in the effective-fluid simulation to the corresponding results obtained in MC simulations of the full binary mixture. We also compare the simulation results to the predictions based on the BPGG integral equation. These simulations were

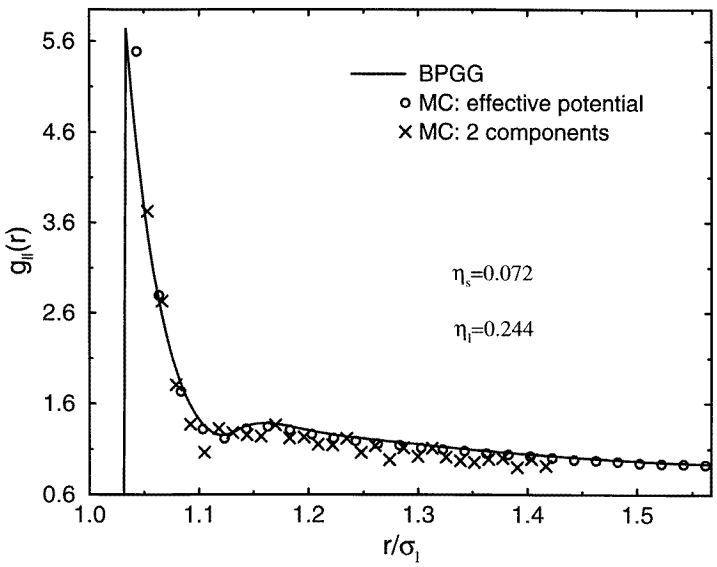

Figure 10. The pair distribution function for the large particles. A comparison of MC data for the effective one-component fluid, MC data for the full binary system and the BPGG integral equation. The calculations were performed at state point 'A' of the phase diagram.

performed at the state point 'A' in the phase diagram of figure 1. We note that the simulations of the effective one-fluid model are in good agreement with the results for the full simulation of the mixture. There is no reason to assume that the remaining discrepancies in figure 10 are due to an inadequacy of the effective one-fluid model. After all, the number of large spheres in the full simulation of the binary mixture is quite small ($\mathcal{O}(10)$) and the statistical accuracy of this simulation is rather poor. Note also that the effective-one-fluid simulation data are in excellent agreement with the BPGG prediction.

Next, we increase the chemical potential of the small particles, in order to increase the depletion effects. To this end, we study state point 'C' of the phase diagram ($\rho_s^* = 0.7\sigma_s^{-3}, \eta_l = 0.1$). Here, we observe very interesting behaviour. In the absence of the depletion potential the system of large (hard) spheres equilibrates in several thousand Monte Carlo cycles (trial moves per particle). If now we switch on the depletion potential, the relaxation of the system to its equilibrium state changes dramatically. Below, we discuss what happens to the pair structure during a fairly long MC simulation (2.5×10^6 Monte Carlo cycles). We shall see that the short-range structure equilibrates quite rapidly (the pressure equilibrium process). In contrast, the equilibration of the large-scale structure is rather slow. We stress, however, that the MC results for the rate of structural relaxation can, at best, be suggestive, as the MC simulation technique does not mimic the real (hydro-) dynamics of the system.

4.1. Short-range structure

Let us first compare the contact value for $g(r)$ as measured in the MC simulations to the predictions of the various integral equations. The PY approximation predicts a value $g^{PY}(\sigma_l^+) \simeq 17.5$, while the BPGG approximation yields $g^{BPGG}(\sigma_l^+) \simeq 90$. The MC results of figure 11 show that $g(r)$ at contact reaches a value that is close to 400. The

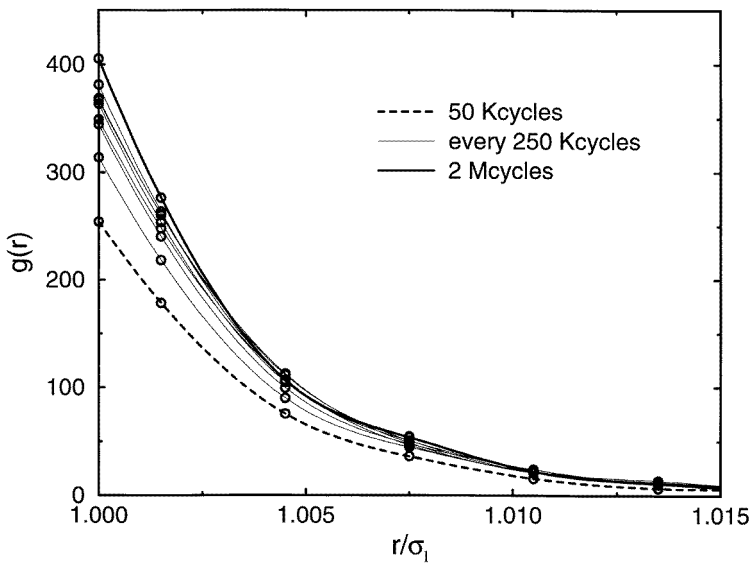

Figure 11. The behaviour of the pair distribution function as a function of MC 'time' for state point 'C'. This figure represents the evolution of the peak in $g(r)$ at contact. The value at contact is based on a quadratic extrapolation. Note that the peak is very narrow (only 5% of the diameter of the small particles). Each curve corresponds to an average over 250 kilocycles.

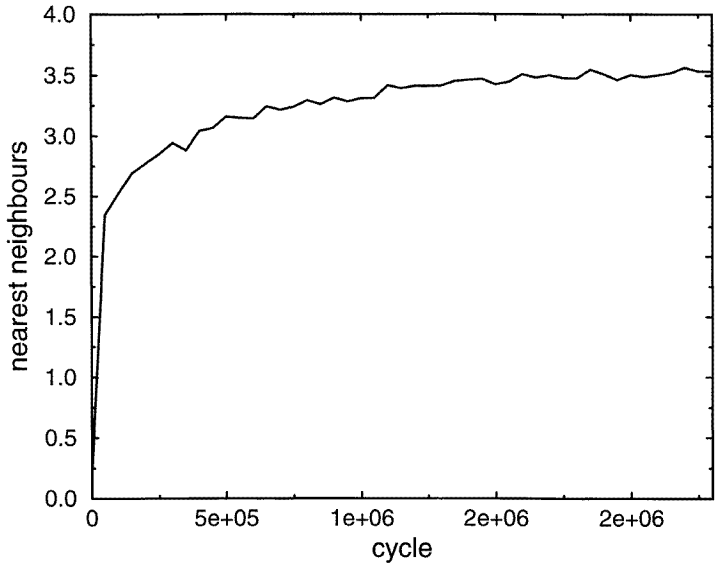

Figure 12. Evolution of the number of nearest neighbours (particles contained in the contact peak of $g(r)$) at state point 'C'. Already during the first few thousand MC cycles there is a strong tendency of the particles to stick.

underestimation of the contact value by the PY approximation is not a surprise, since this is one of the well known defects of that approximation. In contrast, the BPGG approximation

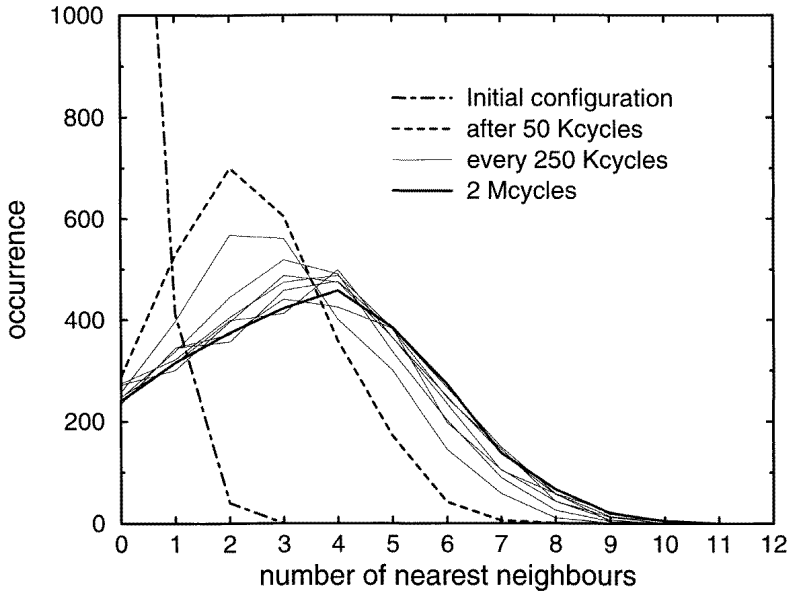

Figure 13. A histogram of the number of nearest neighbours at state point 'C'. The distribution is very wide. This suggests that the structure that develops during the simulation is not (yet) very well ordered.

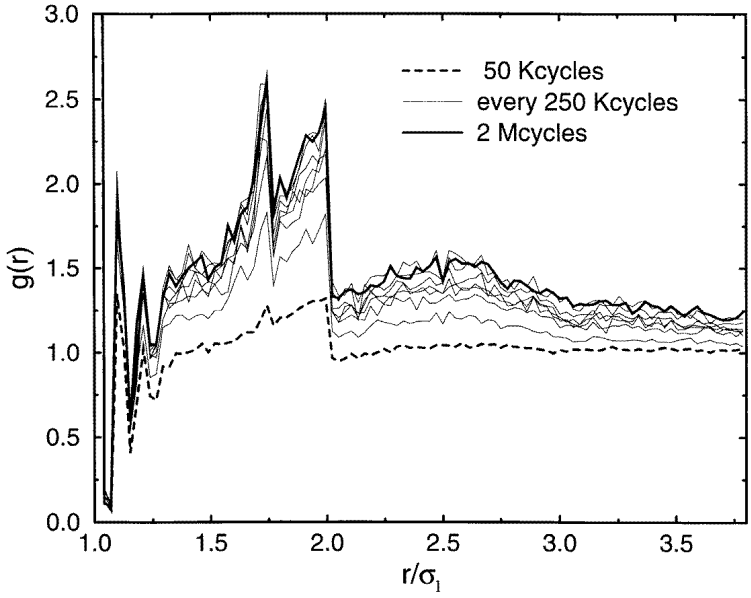

Figure 14. The pair distribution function at state point 'C'. We can observe in this figure the slow relaxation of the local order. It is important to notice that the short-range structure (the contact peak and second peak) do not change much during the simulation. The remarkable point is the emergence of a peak at $r \simeq 1.75\sigma_l$, showing a tendency of the system to create a local order (see the text).

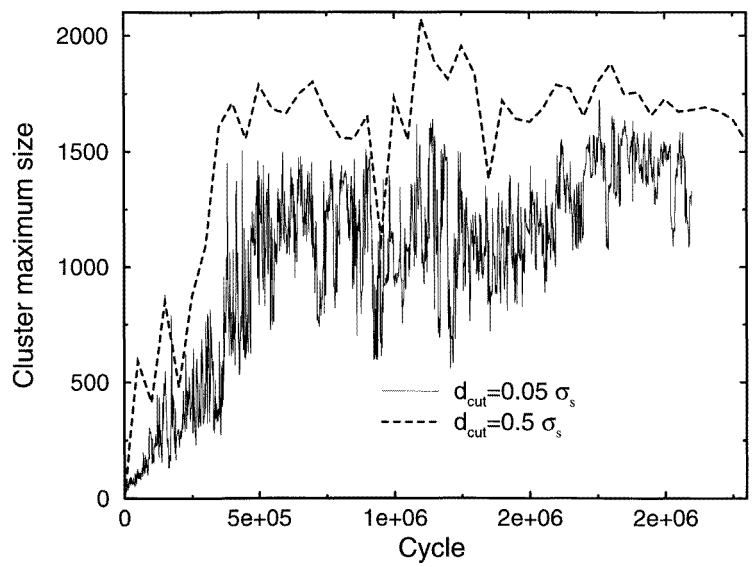

Figure 15. The evolution of the size of the largest cluster at state point 'C'. The two curves correspond to different values of the cut-off used to identify bound particles. After 500 kilocycles, the largest cluster contains half of the particles in the system, and its size does not vary much after that.

usually does much better. But not in this case. Figure 11 shows the evolution of the magnitude of the peak at contact during the MC simulation. The estimated contact values shown in this figure are based on quadratic extrapolations. We observe an increase of the contact value during the simulation, but the very large value of 250 is already reached after some 50 kilocycles. We also stress the very short range of the contact peak, typically less than $0.1\sigma_s$. This very small value of the width of the contact peak is due to the shape of the depletion potential: a very sharp attractive well followed by a rather broad repulsive barrier. The poor performance of the BPGG integral equation is a first sign of the breakdown of these integral equations at extreme size ratios and high densities. Integral equations tend to strongly underestimate the stickiness of colloidal particles. We conclude from MC data that the depletion potential tends to make the particles stick together, and that this process is, at least initially, rather fast. To emphasize this point, we have computed the evolution of the number of nearest neighbours as a function of MC 'time' (figure 12). The number of nearest neighbours is defined as the mean number of particles within a distance corresponding to the width of the first peak of $g(r)$. The cut-off distance that we chose was $d_{cut} = 0.5\sigma_s$. In any event, as the peak of $g(r)$ at contact is very narrow, and the precise choice of d_{cut} is not crucial. The number of neighbours increases very rapidly from zero to 2.5, and then relaxes more slowly to the value of 3.5. Histograms of the number of nearest neighbours are presented in figure 13. Note that, after about 10^6 MC cycles, the system appears to have reached an equilibrium state. If we now consider the organization of next-nearest neighbours (figure 14), we observe a slow reorganization with the appearance of a local peak at a distance $r = \sqrt{3}\sigma_l$, and a discontinuity at $r = 2\sigma_l$. This is precisely the behaviour expected for sticky spheres. The discontinuity at $r = 2\sigma_l$ is reproduced by the PY equation for adhesive spheres [27]. The peak at $r = \sqrt{3}\sigma_l$ is not contained in the PY equation, but is found in MC simulations of the sticky-sphere model [28]: it corresponds

to a local organization of particles into a trigonal bi-pyramid. The only difference is that in the adhesive-sphere limit, this peak is a δ-function peak and the discontinuity at $2\sigma_l$ is a true discontinuity. Here both features are slightly smeared.

In this context, it is interesting to study the clustering of the large spheres. To this end, we need a clustering criterion. In what follows, we consider two particles to belong to the same cluster if their separation is smaller than d_{cut}. In figure 15, we compare the evolution of the largest cluster size for two values of 'd_{cut}', namely $0.5\sigma_s$ and $0.05\sigma_s$. Although the two curves do differ quantitatively, they are qualitatively very similar. And even the quantitative differences between the two curves are not very large. This implies that the typical separation between two neighbouring particles in a cluster is smaller than $0.05\sigma_s = 0.005\sigma_l$! If we now consider the size of the largest cluster, the measured value oscillates around a value of 1500 particles! As the total number of particles in our system is only 2700, it is safe to conclude that, at point 'C', a finite fraction of all particles reside in a percolating cluster. The strong fluctuations that we can observe in both curves of figure 15 are reassuring since they show that the MC algorithm enables the cluster to exchange particles with the rest of the fluid. The observed cluster, although probably meta-stable with respect to the crystalline state, is therefore in dynamic equilibrium with the liquid.

4.2. Large-scale structure

Figures 16 and 17 show the variation of the structure factor of the system at the beginning and the end of the simulation compared to the average over the simulation. The most striking feature is the large peak at low k-values. This is indicative of strong density fluctuations on larger length scales. It provides one more indication that the fluid is, in fact, inhomogeneous. In other words, at state point 'C', the binary mixture of hard spheres appears to undergo spontaneous phase separation. This is the first numerical evidence for such behaviour that was predicted on basis of integral equation predictions [13].

The second point is the tendency towards large-scale ordering that we can observe by looking at the peaks appearing in figure 17. We can understand this property as follows: the fluid first forms large disordered clusters by essentially random adhesion of 'sticky' particles. Subsequently, the structure of the cluster relaxes to a more stable state. However, this relaxation is slow, as the reorganization of a cluster requires bond breaking. The structure factor in figure 17 suggests that the final cluster has appreciable crystalline ordering. However, the peaks that we observe in the structure factor are rapidly fluctuating, which explains that they do not show up quite as strongly in the mean structure factor. In any event, the behaviour that we observe is compatible with a scenario where, in the first stages of the phase separation, the large spheres cluster into an amorphous phase. This amorphous phase subsequently transforms slowly into a phase with appreciable crystalline order. On the time-scale of our simulation, this crystallization is still far from complete.

The final figure (figure 18) shows the osmotic compressibility as estimated from the low-k behaviour of the structure factor:

$$\rho_l k_B T \chi_T = S(k = 0) \tag{24}$$

It is not possible to measure directly the $k = 0$ value in a simulation, since the volume is not fluctuating. We have therefore estimated the $k = 0$ value by extrapolating the data obtained for the two smallest k-values that fit in the periodic box ($L = 24.2\sigma_l$). As can be seen from the figure, the peak at $k = 0$ keeps on growing throughout the simulation, and there is no evidence for its levelling off. This is one more piece of evidence suggesting that a slow phase separation is taking place.

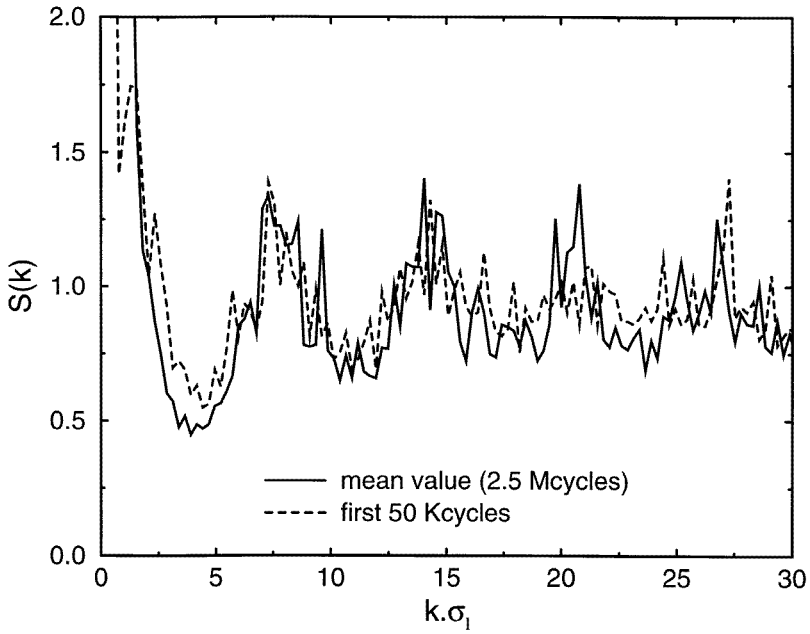

Figure 16. The structure factor at state point 'C'. This figure shows the structure factor at the beginning of the simulation compared to its value averaged all over the two megacycles. For the large-k regime shown here, the two curves are rather similar.

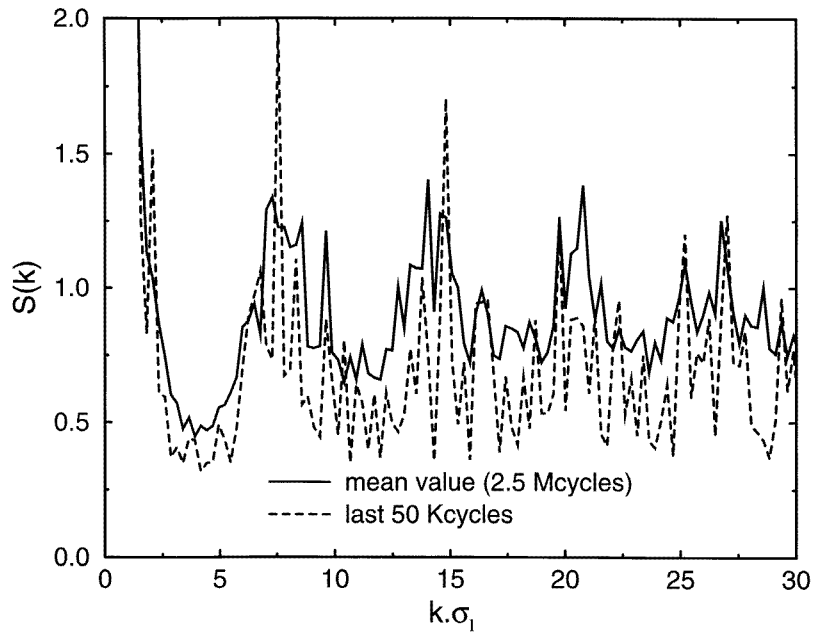

Figure 17. The structure factor at state point 'C'. The structure factor at the end of the simulation compared to the mean value. Some sharp, but fluctuating, peaks appear in the structure, suggesting instantaneous crystalline order. However, no such order is apparent in the averaged curve.

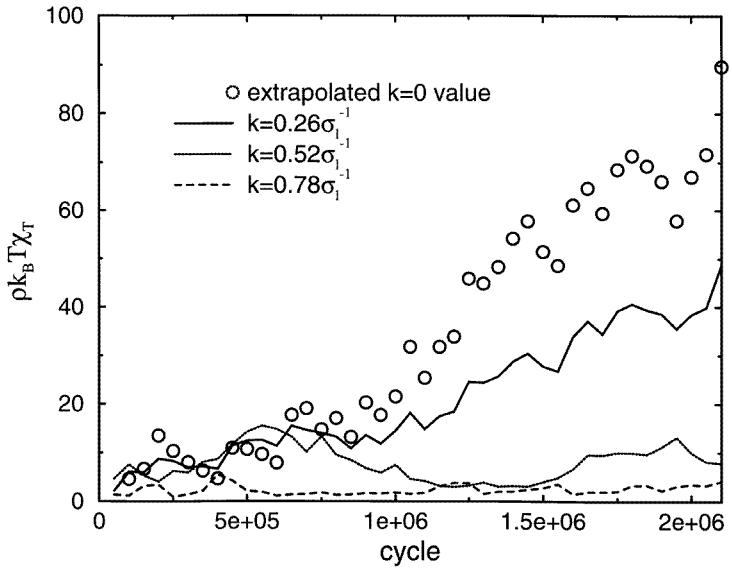

Figure 18. The evolution of the compressibility at state point 'C'. This figure shows the large-scale density fluctuation enhancement during the simulation.

5. Conclusion

The MC data presented in this paper confirm the prediction of integral equations about the spinodal instability of a mixture of large and small spheres. But, although the MC data are, in this respect, in qualitative agreement with the integral equation predictions, there are appreciable quantitative discrepancies. All integral equations tend to underestimate the stickiness of large particles. A detailed study of the effective depletion force showed that whereas the superposition approximation is not able to reproduce the variations of the potential inside the depletion well, the perturbative expression obtained by Mao *et al* [2] does so, even at high density. In contrast, the perturbation theory fails earlier at large inter-particle separations.

The study of the three-particle contribution to the effective force suggests that the model of an effective fluid interacting through a pairwise-additive depletion potential should accurately describe a binary mixture of hard spheres, at least for a size ratio of 0.1 or less. This model has been tested by comparing the pair structure obtained from MC simulations of the full binary system, MC simulations of the effective system and predictions of integral equations.

For one state point, we find that the mixture exhibits a clear tendency to phase separate. This effect shows up in the behaviour of the structure factor at small k-values. But the phase separation is rather different from that found in simple liquids, since it results in the growth of huge clusters involving a large fraction of all of the particles in the system. Such behaviour is reminiscent of phase separation in the adhesive hard-sphere system. We can observe two steps in the cluster growth: during the first step the particles rapidly stick together, more or less at random. During the second step the structure of the cluster relaxes. This is a slow process that has not yet been characterized very well, but both the pair distribution function and the structure factor show indications of local ordering. As

the cluster relaxation is very slow, we are probably only probing the early stages of this process.

A comparison of our numerical results with experimental data is quite difficult, since most experimental colloidal mixtures behave like slightly non-additive hard-sphere mixtures. However, it is tempting to compare our results to the experiments performed by van Duijneveldt *et al* [29], who observed a spinodal instability in a mixture of hard-sphere-like colloidal particles, that present the same characteristics as those observed in MC simulations (very slow dynamics and no clear long-range order on the time-scale of the experiment).

In any event, it would be very interesting to study the later stages of the cluster relaxation, using techniques that are more sensitive to various forms of crystalline order. An obvious probe to use in a simulation would be the study of the bond orientational order.

Acknowledgments

The authors thank H N W Lekkerkerker for many stimulating discussions. The work of the FOM Institute is part of the scientific programme of the FOM and is supported by the Nederlandse Organisatie voor Wetenschappelijk Onderzoek (NWO).

Appendix A

The algorithm used to perform the MC simulations for the full binary system is the following.

The move of a small particle is performed according to the standard MC algorithm for hard spheres. A trial move of a large particle consists in the following steps.

(1) A new position $\boldsymbol{r}_{new}$ is chosen around the 'old' position $\boldsymbol{r}_{old}$ of the large particle. This new position is chosen at random in a cubic box centred on $\boldsymbol{r}_{old}$. The size of the box is a fraction of the diameter of the large particles. As a consequence, the large particle placed at its new position overlaps many small particles, and possibly large ones.

(2) In the case of an overlap with another large particle, the move is automatically rejected.

(3) Otherwise, small particles overlapping the large sphere placed at its new position are identified. These particles have their centres in a sphere of radius ξ centred at $\boldsymbol{r}_{new}$.

(4) The next step consists in the insertion of these small particles into the volume left by the move of the large one: a sphere of radius ξ centred at $\boldsymbol{r}_{old}$. The algorithm used to perform the insertion is derived from the procedure proposed by Siepmann and Frenkel [15, 16] for polymer simulation. The only difference is the random choice of trial positions in the insertion volume.

References

[1] Asakura S and Oosawa F 1958 *J. Polym. Sci.* **33** 183
[2] Mao Y, Cates M E and Lekkerkerker H N W 1995 *Physica* A **222** 10
[3] Horn R G and Israelachvili J N 1981 *J. Chem. Phys.* **75** 1400
[4] Gazzillo D 1991 *J. Chem. Phys.* **95** 4565 and references therein
[5] Biben T and Hansen J-P 1997 *Physica* A at press
[6] Barboy B and Gelbart W M 1979 *J. Chem. Phys.* **71** 3053
[7] Ornstein L S and Zernike F 1914 *Proc. Akad. Sci. (Amsterdam)* **17** 793
[8] Percus S K and Yevick G J 1958 *Phys. Rev.* **110** 1
[9] Rogers F J and Young D A 1984 *Phys. Rev.* A **30** 999
[10] Ballone P, Pastore G, Galli G and Gazzillo D 1986 *Mol. Phys.* **59** 275
[11] Biben T 1993 *PhD Thesis* Université Claude Bernard-Lyon I, France

[12] Biben T and Hansen J-P 1990 *Europhys. Lett.* **12** 347
[13] Biben T and Hansen J-P 1991 *Phys. Rev. Lett.* **66** 2215
[14] Heno Y and Regnaut C 1991 *J. Chem. Phys.* **95** 9204
[15] Siepmann J I and Frenkel D 1992 *Mol. Phys.* **75** 59
[16] Frenkel D, Mooij G C A M and Smit B 1991 *J. Phys.: Condens. Matter* **3** 3053
[17] Dijkstra M and Frenkel D 1994 *Phys. Rev. Lett.* **72** 298
[18] Dijkstra M, Frenkel D and Hansen J-P 1994 *J. Chem. Phys.* **101** 3179
[19] Bolhuis P G and Frenkel D 1994 *J. Chem. Phys.* **101** 9869
[20] Lebowitz J L 1964 *Phys. Rev.* A **133** 895
[21] Lebowitz J L and Rowlinson J S 1964 *J. Chem. Phys.* **41** 133
[22] Piasecki J, Bocquet L and Hansen J-P 1995 *Physica* A **218** 125
[23] Attard P 1989 *J. Chem. Phys.* **91** 3072, 3083
[24] Widom B 1963 *J. Chem. Phys.* **39** 2808
[25] Lebowitz J L, Helfand E and Praestgaard E 1965 *J. Chem. Phys.* **43** 774
[26] Lekkerkerker H N W 1990 *Colloids Surf.* **51** 419
[27] Baxter R J 1968 *J. Chem. Phys.* **49** 2770
[28] Kranendonk W G T and Frenkel D 1988 *Mol. Phys.* **64** 403
[29] van Duijneveldt J S, Heinen A W and Lekkerkerker H N W 1993 *Europhys. Lett.* **21** 369